RESEARCH ARTICLE

Dynamics of β-Adrenergic/cAMP Signaling and Morphological Changes in Cultured Astrocytes

Nina Vardjan,[1,2] Marko Kreft,[1,2,3] and Robert Zorec[1,2]

The morphology of astrocytes, likely regulated by cAMP, determines the structural association between astrocytes and the synapse, consequently modulating synaptic function. β-Adrenergic receptors (β-AR), which increase cytosolic cAMP concentration ($[cAMP]_i$), may affect cell morphology. However, the real-time dynamics of β-AR-mediated cAMP signaling in single live astrocytes and its effect on cell morphology have not been studied. We used the fluorescence resonance energy transfer (FRET)-based cAMP biosensor Epac1-camps to study time-dependent changes in $[cAMP]_i$; morphological changes in primary rat astrocytes were monitored by real-time confocal microscopy. Stimulation of β-AR by adrenaline, noradrenaline, and isoprenaline, a specific agonist of β-AR, rapidly increased $[cAMP]_i$ (∼15 s). The FRET signal response, mediated via β-AR, was faster than in the presence of forskolin (twofold) and dibutyryl-cAMP (>35-fold), which directly activate adenylyl cyclase and Epac1-camps, respectively, likely due to slow entry of these agents into the cytosol. Oscillations in $[cAMP]_i$ have not been recorded, indicating that cAMP-dependent processes operate in a slow time domain. Most Epac1-camps expressing astrocytes revealed a morphological change upon β-AR activation and attained a stellate morphology within 1 h. The morphological changes exhibited a bell-shaped dependency on $[cAMP]_i$. The 5–10% decrease in cell cross-sectional area and the 30–50% increase in cell perimeter are likely due to withdrawal of the cytoplasm to the perinuclear region and the appearance of protrusions on the surface of astrocytes. Because astrocyte processes ensheath neurons, β-AR/cAMP-mediated morphological changes can modify the geometry of the extracellular space, affecting synaptic, neuronal, and astrocyte functions in health and disease.

GLIA 2014;62:566–579

Key words: astrocytes, β-adrenergic signaling, fluorescence resonance energy transfer, cAMP, stellation

Introduction

Astrocytes, the most abundant glial cells in the mammalian central nervous system (CNS), exhibit a special form of excitability, characterized by elevations in the cytosolic free Ca^{2+} concentration ($[Ca^{2+}]_i$), which are elicited by various transmitters and chemical messengers (Guček et al., 2012; Parpura et al., 2012; Zorec et al., 2012). In addition to the second messenger Ca^{2+}, cyclic adenosine monophosphate [cAMP; (Sutherland and Rall, 1960)] modulates a large variety of cellular functions and regulates numerous biological processes in astrocytes (Allaman et al., 2003; Balázs et al., 1998; Bolton et al., 2006; Ciccarelli et al., 2007; Durand et al., 2011; Kanno and Nishizaki, 2012; Kreft et al., 2012; Rathbone et al., 1991; Sorg and Magistretti, 1992; Yu et al., 1993).

cAMP synthesis is mainly triggered by agonist-induced activation of transmembrane G protein-coupled receptors (GPCRs) and subsequent activation of adenylyl cyclases (ACs) at the inner site of the plasma membrane. cAMP activates a number of effectors in the cell, primarily the cAMP-dependent protein kinase (PKA) which, by phosphorylating cytoplasmic and nuclear targets, mediates many different functional effects (Beavo and Brunton, 2002), although signaling via cAMP-activated GTP-exchange protein (Epac) (de Rooij et al., 1998) and via cAMP-gated ion channels is also present. The cellular content of cAMP is tightly controlled by GPCRs via both ACs and cAMP-degrading phosphodiesterases (PDEs) (Beavo and Brunton, 2002).

Astrocytes express several types of GPCRs (e.g., β-adrenergic receptors [β-AR], metabotropic glutamate

View this article online at wileyonlinelibrary.com. DOI: 10.1002/glia.22626

Published online January 24, 2014 in Wiley Online Library (wileyonlinelibrary.com). Received July 19, 2013, Accepted for publication Dec 20, 2013.

Address correspondence to Robert Zorec, Institute of Pathophysiology, Faculty of Medicine, University of Ljubljana, Zaloška 4, Ljubljana, Slovenia. E-mail: robert.zorec@mf.uni-lj.si

From the [1]Celica Biomedical Center, Tehnološki Park 24, Ljubljana, Slovenia; [2]Laboratory of Neuroendocrinology-Molecular Cell Physiology, Institute of Pathophysiology, Faculty of Medicine, University of Ljubljana, Zaloška 4, Ljubljana, Slovenia; [3]Biotechnical Faculty, University of Ljubljana, Večna Pot 111, Ljubljana, Slovenia.

receptors, and adenosine receptors). β-ARs are abundantly present on astrocytes in both white and grey matter of the brain (Aoki, 1992; Catus et al., 2011; Sutin and Shao, 1992; Zeinstra et al., 2000) and regulate important astrocyte functions via activation/inhibition of cAMP-dependent pathways. Activation of the β-AR/cAMP signaling pathway in astrocytes by the fight or flight response neurotransmitter noradrenaline (NA) has been shown to promote rapid degradation of glycogen in astrocytes, which serves as the main energy reserve in the brain (Kreft et al., 2012; Prebil et al., 2011a). NA may also affect cytosolic glucose availability via β-AR/cAMP signaling (Kreft et al., 2012; Prebil et al., 2011b; Yu et al., 1993) and increase glycogen content (Allaman et al., 2003; Sorg and Magistretti, 1992). β-AR stimulation can induce the expression of cytokine IL-6 in astrocytes (Norris and Benveniste, 1993) and neurotrophic factors (Schwartz and Nishiyama, 1994), modulate glial inwardly rectifying potassium channels (Kir) (Roy and Sontheimer, 1995), and modulate the extracellular concentration of adenosine (Rosenberg and Li, 1995) and glutamate (Aoki, 1992). Moreover, impaired regulation of the astrocytic β_2-AR/cAMP pathway is considered to contribute to the pathophysiology of several neurologic conditions such as multiple sclerosis (Laureys et al., 2010) and Alzheimer's disease (Lee et al., 1997). Astroglial β-ARs also functionally regulate astrocyte cellular morphology (Hatton et al., 1991). An increase in intracellular cAMP production on β-AR stimulation induces astrocyte stellation, that is, transformation from a flattened irregular morphology to a stellate, process-bearing morphology (Bicknell et al., 1989; Shain et al., 1987).

However, the real-time dynamics of β-AR-mediated cAMP signaling in live single astrocyte has not been studied yet in detail. Moreover, it is also unclear how the activation of β-ARs affects astrocyte morphology. Genetically encoded fluorescence resonance energy transfer (FRET) biosensors that enable direct monitoring of rapid changes in free cytosolic cAMP were developed recently (Willoughby and Cooper, 2008). These sensors are based on downstream cAMP targets, including cAMP-dependent PKA (Zaccolo et al., 2000; Zhang et al., 2001, 2005), cAMP-gated ion channels (Nikolaev et al., 2006; Rich et al., 2001), and Epac (DiPilato et al., 2004; Nikolaev et al., 2004). In this study, we used the FRET-based cAMP biosensor, Epac1-camps (Nikolaev et al., 2004), and real-time confocal imaging to study temporal cytosol cAMP dynamics; cell morphology was monitored by measuring cell cross-sectional area and perimeter in primary rat astrocytes on β-AR stimulation or activation of the cAMP signaling pathway downstream of the β-AR.

The experimental evidence revealed that, in astrocytes, β-AR agonists induce a rapid increase in $[cAMP]_i$, as measured by the 10–15% change in the FRET ratio with a time constant of ∼15 s. However, oscillations in the time-dependent changes in $[cAMP]_i$ have not been observed in any study on astrocytes. The effect of adrenaline (ADR) on cytosolic cAMP levels was concentration dependent with a half-maximal response obtained at ∼30 nM ADR. Within an hour, this stimulation resulted in a 5–10% decrease in cell cross-sectional area and a 30–50% increase in the cell perimeter. The relationship between the amplitude of the FRET signal, reflecting the $[cAMP]_i$, and the change in astrocyte cell cross-sectional area and perimeter presented a bell-shaped curve. The physiologic and pathological implications of these results are considered in the discussion.

Abbreviations

AC	adenylyl cyclase
ADR	adrenaline
ANOVA	one-way analysis of variance
β-AR	beta-adrenergic receptor
cAMP	3′–5′-cyclic adenosine monophosphate
CFP, YFP	enhanced cyan and yellow fluorescent proteins, respectively
CSF	cell shape factor
db-cAMP	dibutyryl-cAMP
DAPI	4′,6-diamidino-2-phenylindole
DDA	2′,5′-dideoxiadenosine
Epac	exchange protein directly activated by cAMP
FRET	fluorescence resonance energy transfer
FSK	forskolin
GFAP	glial fibrillary acidic protein
GPCR	G protein-coupled receptor
GS	glutamine synthetase
IBMX	3-isobutyl-l-methylxanthine
Iso	isoprenaline
NA	noradrenaline
PDE	phosphodiesterase
PKA	protein kinase A
Pro	propranolol

Materials and Methods

Cell Culture and Reagents

Astrocytes from the cortex of 2–3-day-old rats (Wistar) were isolated as described (Schwartz and Wilson, 1992). Before the experiments, the cells were removed from the culture flasks with trypsin/EDTA and plated on 22-mm diameter glass cover slips coated with poly-L-lysine. Cells were maintained in high-glucose Dulbecco's modified Eagle's medium (DMEM) supplemented with 10% fetal bovine serum, 1 mM sodium pyruvate, 2 mM L-glutamine, and 25 μg/ml penicillin–streptomycin in an atmosphere of humidified air (95%) and CO_2 (5%). The purity of the astrocyte cultures was determined immunocytochemically using antibodies against astrocytic markers, glial fibrillary acidic protein (GFAP), or glutamine synthetase (GS; Abcam, Cambridge, UK). Astrocytes were transfected using FuGENE® 6 Transfection Reagent (Promega Corporation, Madison, WI). The viability of astrocytes after transfection was determined by LIVE/DEAD® Viability/Cytotoxicity Kit (Molecular Probes, Invitrogen, Eugene, OR). All chemicals were from Sigma Aldrich (St. Louis, MO) unless otherwise noted.

The experimental animals were cared for in accordance with the International Guiding Principles for Biomedical Research Involving Animals developed by the Council for International Organizations of Medical Sciences and Animal Protection Act (Official Gazette of the RS, No. 38/13).

Immunostaining

Astrocytes growing on the cover slips and expressing the Epac1-camps FRET construct (Nikolaev et al., 2004) were fixed using 4% paraformaldehyde in phosphate buffer saline for 10 min at room temperature before being treated with 10% goat serum for 1 h at 37°C. Cultures were then stained with primary mouse anti-GFAP antibodies for 2 h at 37°C (1:250 dilution). After washing to remove excess primary antibody, the cultures were incubated for 1 h at 37°C with Alexa Fluor^{546} conjugated secondary goat anti-rabbit IgG (1:600 dilution; Abcam, Cambridge, UK). Excess antibody was removed and the cells were labeled with 4,6-diamidino-2-phenylindole (DAPI) according to the manufacturer's instructions (Molecular Probes, Invitrogen, Eugene, OR) and treated with SlowFade Gold antifade reagent (Molecular Probes, Invitrogen, Eugene, OR). Immunolabeled cells were imaged with an inverted Zeiss LSM780 confocal microscope with an oil immersion plan apochromatic objective (63×, 1.4 NA; Carl Zeiss, Jena, Germany) using 488-nm Ar-ion, 543-nm He–Ne, and 405-nm diode laser excitation. Emission spectra were acquired sequentially with a 505–530-nm bandpass emission filter (Alexa Fluor^{488}), a 560-nm long-pass emission filter (Alexa Fluor^{546}), and a 445–450-nm bandpass filter (DAPI).

FRET Measurements and Analysis

Astrocytes expressing the Epac1-camps FRET construct were examined with a Plan NeoFluoar 40×/1.3 oil DIC immersion objective (Carl Zeiss, Jena, Germany) and a twofold zoom factor using a Zeiss LSM510 META confocal microscope (Carl Zeiss, Jena, Germany). Cells were excited at 458 nm and images (512 × 512) were acquired every 3.5 s or 7 s using lambda stack acquisition. Emission spectra were collected from a META detector in eight channels (lambda stack) ranging from 470 to 545 nm, each with a 10.7-nm width. Two-channel (cyan fluorescent protein [CFP] and yellow fluorescent protein [YFP]) images were generated from lambda stacks by analytical software, Extract channels. Channels with emission spectra at 470 and 481 nm and emission spectra at 513, 524, and 534 nm were extracted to the CFP channel and YFP channels, respectively. YFP and CFP fluorescence intensities were quantified within a region of interest (ROI) selected for individual cells expressing Epac1-camps using LSM 510 META software. In the graphs, the FRET signal is reported as the ratio of the YFP to CFP fluorescence signal after subtracting the background fluorescence from both YFP and CFP signals using SigmaPlot. The values of the FRET signals were normalized (set to 1.0) at the onset of the experiments. A decrease in the FRET signals reflects an increase in $[cAMP]_i$.

Initially, astrocytes were kept in standard extracellular solution (10 mM Hepes/NaOH, pH 7.2, 10 mM D-glucose, 131.8 mM NaCl, 1.8 mM $CaCl_2$, 2 mM $MgCl_2$, and 5 mM KCl) and then treated with various reagents following a 100-s baseline: 50 μM forskolin (FSK), 200 μM 3-isobutyl-L-methylxanthine (IBMX; a nonspecific inhibitor of cAMP PDEs), 1 mM dibutyryl-cAMP (db-cAMP; a membrane-permeable derivative of cAMP), 100 μM 2′,5′-dideoxiadenosine (DDA; AC inhibitor), 1 μM ADR (α- and β-adrenergic receptor agonist), 1 μM noradrenaline (NA; α- and β-adrenergic receptor agonist), 1 μM isoprenaline (Iso; β-adrenergic receptor agonist), and 1 μM propranolol (Pro; a β-adrenergic receptor antagonist).

Statistical Analysis

The changes in the YFP/CFP fluorescence emission ratio were normalized to baseline ratio values. Single-exponential ($F = F_0 + c \times \exp(-t/\tau)$) decay functions or single-exponential increase to maximum functions ($F = F_0 + c \times (1 - \exp(-t/\tau))$) were fitted to the diagrams with YFP/CFP fluorescence emission ratios using SigmaPlot. The time constant (τ) and the YFP/CFP emission ratio amplitudes (c) were determined from the fitted curves. F is the YFP/CFP emission ratio at time t, F_0 is the baseline YFP/CFP emission ratio, c is YFP/CFP emission ratio amplitude of $F_{(t\,=\,0)} - F_0$, and τ is the time constant of the individual exponential component. The goodness of the exponential fits was judged from the calculated coefficient of determination, R^2.

In dose-dependence studies, the maximum YFP/CFP ratio response was calculated by subtracting the mean YFP/CFP ratio measured during the last 100 s after stimulation from the mean YFP/CFP ratio measured during the first 100 s before stimulation (baseline). An average of the maximum YFP/CFP emission ratio response was determined for each concentration of ADR. The four-parameter logistic equation

$$y = \frac{y_{\min} + (y_{\max} - y_{\min})}{1 + (x/\mathrm{EC}_{50})^{-\mathrm{Hillslope}}}$$

was used to fit the dose-dependent curve in SigmaPlot (Systat Software) and to determine the median effective concentration (EC_{50}) value. y_{min} is the minimum response (bottom of the curve), y_{max} is the maximum response (top of the curve), and the Hill slope characterizes the slope of the curve at its midpoint.

LSM 510 META software was used to measure the cell cross-sectional area and the perimeter of isolated Epac1-camps-positive astrocytes before and after treatment of the cells with different reagents. Epac1-positive astrocytes that overlapped significantly with neighboring cells were excluded from the analysis.

A Gaussian three-parameter equation was used to fit the bell-shaped curves to the correlation diagrams between the maximum FRET response *versus* the decrease in cell cross-sectional area or *versus* the increase in cell perimeter, and *versus* cell shape factor (CSF):

$$y = a \times \exp\left(-0.5 \times \frac{(x - x_0)}{b^2}\right).$$

The data of relationship between the increase in cell perimeter and the decrease in cell cross-section area were fitted to the linear function of the form: y (% increase in cell perimeter) $= a + b \times x$

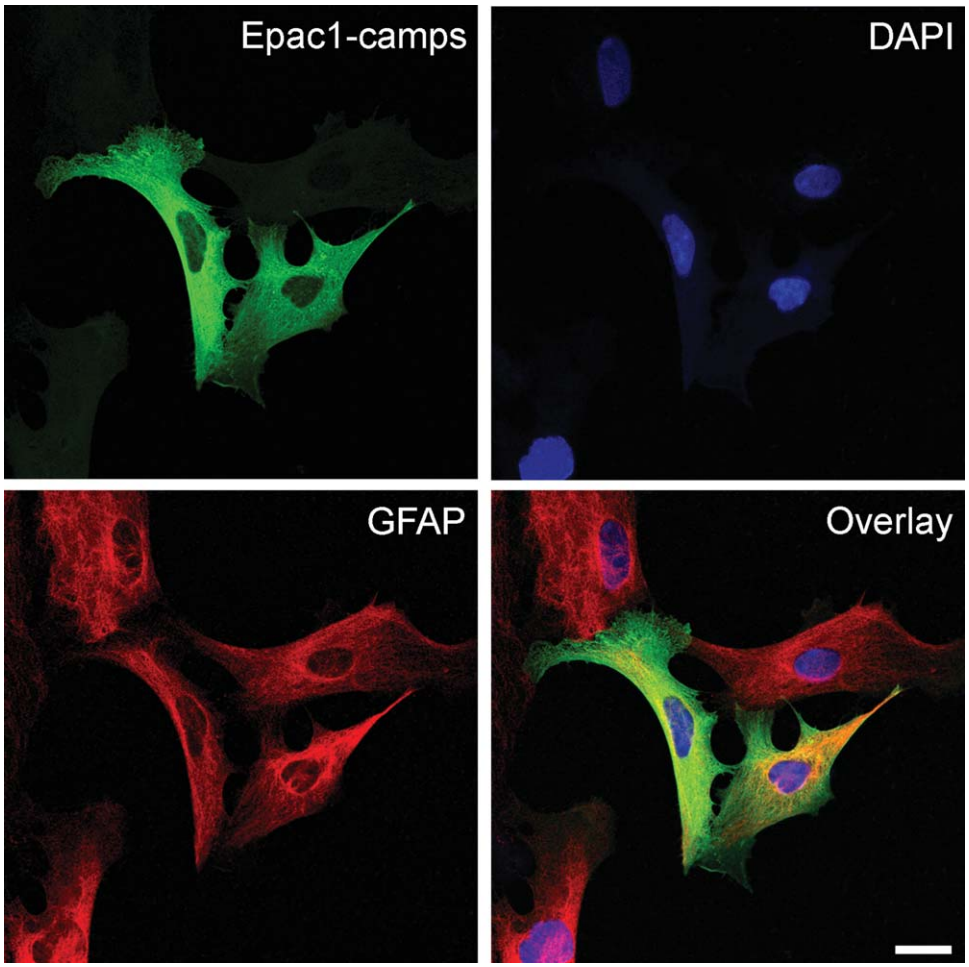

FIGURE 1: Expression of Epac1-camps in primary rat astrocytes. Representative fluorescence images of astrocytes 36 h after transfection with the Epac1-camps FRET pDNA construct. Astrocytes were labeled with DAPI, blue fluorescent nuclear DNA dye, fixed, and immunostained with antibodies against the astrocytic marker GFAP. The merged image (overlay) shows that two of five GFAP-positive cells (red) express Epac1-camps (green). Note that the cAMP reporter is distributed evenly throughout the cytosol, but is excluded from the nucleus. Scale bar: 20 μm.

(% decrease in cell cross-section area), where a represents the intercept and b the slope of the line.

Student's t-test and one-way analysis of variance (ANOVA) between two groups or more than two groups, respectively, were performed to determine statistical significance. ANOVA was followed by pairwise multiple comparison test between groups using a Holm–Sidak method. $P < 0.05$ was considered to be significant.

Results

Properties of Epac1-camps cAMP Nanosensor Expression in Cultured Rat Astrocytes

To image the dynamic changes in free intracellular cAMP in a single living astrocyte, we transfected cells with the FRET-based cAMP sensor Epac1-camps with a single cAMP binding site (Nikolaev et al., 2004). Epac1-camps expression resulted in a uniformly distributed fluorescence throughout the cytosol of transfected astrocytes (Fig. 1). The fluorescence from an individual astrocyte was detected at 16–24 h after transfection. The average percentage of Epac1-camps-positive cells 24 h and 48 h after transfection did not differ significantly (4.8 ± 0.5% *vs.* 4.3 ± 0.5%, respectively; Student's t-test, $P = 0.46$). The mortality of cells transfected with Epac1-camps was higher than in control cells (7.8 ± 1.1% *vs.* 15.6 ± 1.9% and 4.5 ± 0.5% *vs.* 15.8 ± 1.8% [Student's t-test, $P < 0.05$], 24 h and 48 h after transfection), but did not increase within 48 h after transfection (15.6 ± 1.9% *vs.* 15.8 ± 1.8%, respectively; Student's t-test, $P = 0.92$). To evaluate the Epac1-camps sensor in transfected astrocytes, we stimulated cells with the cAMP-increasing membrane-permeable reagent forskolin (FSK), which activates the enzyme AC and increases the intracellular levels of cAMP (Fig. 2). The FRET ratio, determined between CFP (FRET donor) and YFP (FRET acceptor) in Epac1-camps sensor-positive astrocytes, was measured by confocal microscopy using a

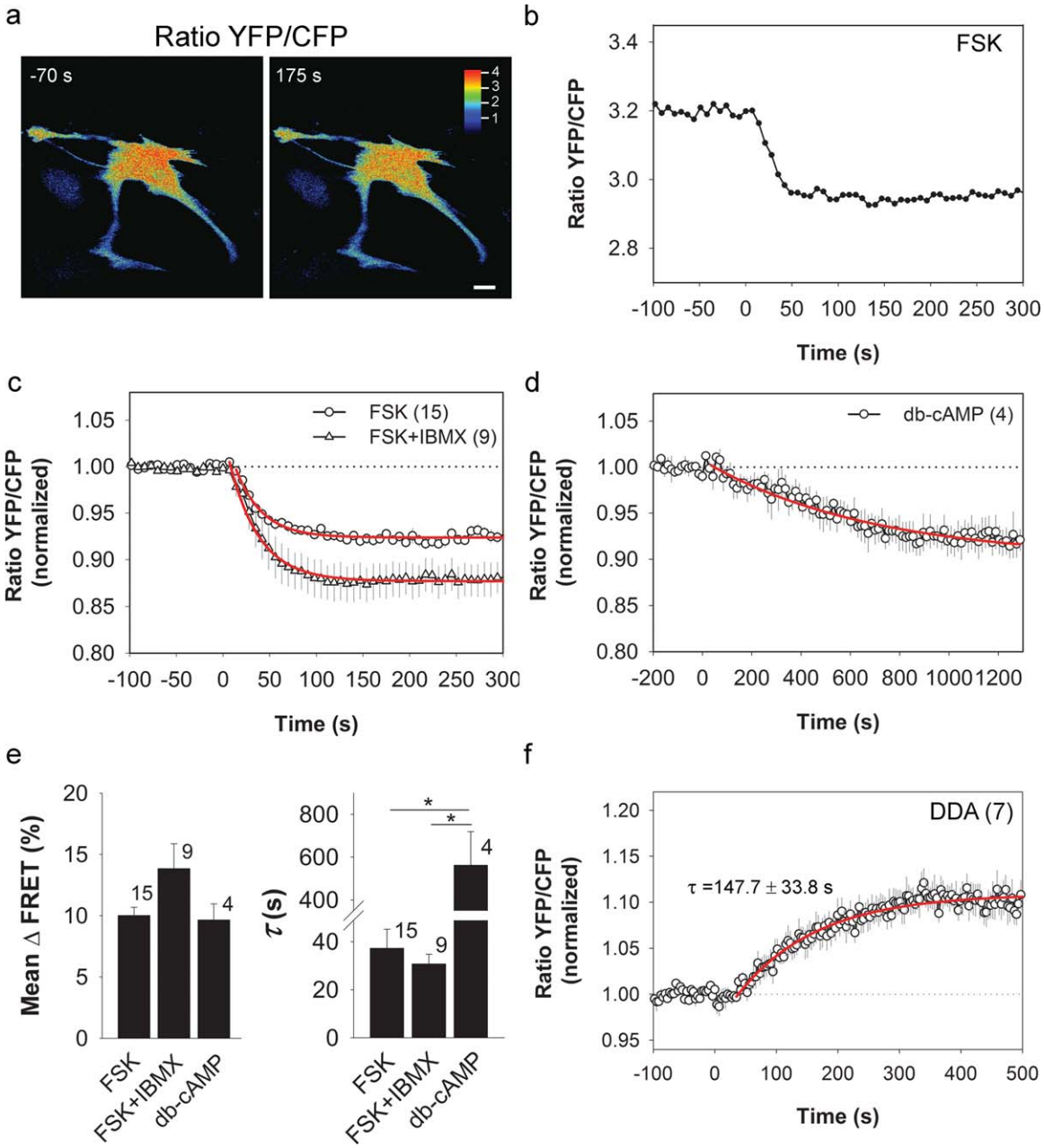

FIGURE 2: Epac1-camps responds to cAMP-increasing agents in astrocytes. (a) Pseudocolor FRET emission ratio images before (−70 s) and after (175 s) the addition of FSK with the corresponding pseudocolor scale bar that depicts the YFP/CFP ratio values. (b) Time course of the Epac1-camps emission ratio recorded in a cell shown in (a) after stimulation with 50 μM FSK. Note the rapid monophasic decline in the FRET signal (represented by the YFP/CFP ratio) after FSK stimulation, reflecting the increase in intracellular cAMP levels. (c, d, f) Time course of the average Epac1-camps emission ratio after the addition of (c) 50 μM FSK, 50 μM FSK with 200 μM IBMX (FSK + IBMX), (d) 1 mM db-cAMP, and (f) 100 μM DDA, an AC inhibitor, at $t = 0$. Data are expressed as the YFP/CFP fluorescence emission ratio normalized to the baseline ratio values (ratio YFP/CFP). The numbers in parentheses depict the number of independent experiments. Single-exponential decay/increase functions were fitted to the curves. (e) Mean amplitude of the changes in Epac1-camps FRET (left) and decay time constants τ (right) for FSK, FSK with IBMX, and db-cAMP. Changes in FRET are expressed as percentages relative to the initial values. $^{*}P < 0.05$ one-way ANOVA comparison between different types of stimuli. Note that the addition of the PDE inhibitor IBMX increased the Epac1-camps response to FSK, an AC activator. Data shown are in the format mean ± SEM. Scale bar: 20 μm.

polychromatic multichannel META detector that enables spectral separation of emitted light. The addition of 50 μM FSK triggered a decrease in the FRET donor/acceptor ratio (Fig. 2a,b). This is consistent with the characteristics of the Epac1-cAMP sensor, which reports the increase in the intracellular cAMP concentration as a decline in the FRET ratio (Nikolaev et al., 2004). Specifically, binding of cAMP to the Epac1-cAMP sensor triggers a conformational change in the

sensor, which increases the distance between CFP and YFP. The average measured Epac1-camps FRET change in response to FSK was 10.02 ± 0.66% (n = 15; Fig. 2c,e). Simultaneous treatment of cells with 50 μM FSK and 200 μM IBMX, which is a nonselective inhibitor of the cyclic nucleotide-degrading enzyme PDE, leads to a larger decrease in the FRET ratio (13.84 ± 2.03% *vs.* 10.02 ± 0.66%; n = 9) compared with FSK alone (Fig. 2c,e).

The time course of the change in the FSK-induced FRET ratio was comparable with the time course of the change in the FSK/IBMX-induced FRET ratio; the time constants (τ) were 37.31 ± 7.98 s and 30.74 ± 4.09 s, respectively (Fig. 2e). Furthermore, to prove that the Epac1-cAMP sensor, when expressed in astrocytes, is activated by direct binding of cAMP molecules, we treated cells with 1 mM membrane-permeable cAMP analog, db-cAMP (Fig. 2d). Stimulation with db-cAMP led to a 9.65 ± 1.31% change in FRET (Fig. 2e), comparable with FSK stimulation. However, the time course of the db-cAMP-induced change in FRET was significantly slower (τ = 562.50 ± 157.29 s, n = 4) compared with cells treated with FSK and FSK/IBMX (one-way ANOVA, $P < 0.05$; Fig. 2e), presumably due to slow permeation of db-cAMP through the plasma membrane (Schultz et al., 1994; Zhang et al., 2001). In two of six cells, the change in the FRET ratio signal appeared with a delay and these cells were not included in the analysis.

To test whether basal cAMP levels in astrocytes can be suppressed by the inhibition of AC, we added 100 μM DDA, an AC inhibitor, to astrocytes expressing Epac1-camps. The addition of DDA increased the change in the FRET ratio by 12.80 ± 1.61% (n = 7) with τ = 147.72 ± 33.80 s (Fig. 2f), likely reflecting a slow decrease in basal cAMP levels. The DDA-induced increase in the change in the FRET ratio occurred with an average delay of ~40 s, likely due to the slow permeation of DDA through the plasma membrane. In seven DDA-treated cells, no significant change in the FRET ratio signal was observed.

Dynamic Changes of cAMP in Astrocytes After Adrenergic Stimulation

To test whether Epac1-camps reports the activation of astrocytic β-ARs (Sutin and Shao, 1992) and subsequent intracellular cAMP increases, we stimulated cultured astrocytes with nonselective β-AR agonists, ADR and NA, and with the selective β-AR agonist, Iso (Fig. 3). The addition of β-AR agonists produced an increase in cAMP with a 10–15% change in the Epac1-camps FRET ratio (Fig. 3d). These changes in FRET had time constants of 13.8 ± 2.5 s (n = 15), 19.8 ± 2.4 s (n = 16), and 18.8 ± 3.9 s (n = 7) for ADR, NA, and Iso, respectively (Fig. 3d). The calculated time constants are approximately twofold smaller compared with the time constants obtained for membrane-permeable cAMP-increasing reagents FSK and FSK/IBMX (Fig. 2e; one-way ANOVA, $P < 0.05$). Within the time resolution of these experiments, there was no evident lag phase between the addition of the AR agonists and the change in the FRET ratio signal. When the cells were pretreated with 1 μM Pro, a β-AR antagonist, the effect of ADR was completely abolished. Pro did not cause any significant effect on the Epac1-camps FRET ratio *per se* (data not shown). The average time constant of the ADR-induced decrease in the FRET ratio in cells pretreated with DDA was approximately fourfold slower than control untreated cells (τ = 56.4 ± 9.5 s [n = 10] *vs.* 13.8 ± 2.5 s, respectively; Fig. 3a), implicating that AC has a role in these processes. To see whether the response of the Epac1-camps FRET ratio to ADR in astrocytes is dose dependent, we treated astrocytes with different concentrations of ADR (Fig. 3e). Figure 3f shows the concentration–response relation to ADR with an EC_{50} value of 29 ± 0.10 nM, which is characteristic of β-AR (Nikolaev et al., 2004).

Effect of Adrenergic Receptor Agonists on Astrocyte Cell Cross-sectional Area and Perimeter

Cultured astrocytes display a flat, fibroblast-like polygonal-shaped morphology. However, an increase in intracellular cAMP levels due to activation of β-ARs may elicit stellation of astrocytes (Lim et al., 1973; Shapiro, 1973), characterized by a star-like shape, resembling the morphology present in the tissue (Shain et al., 1987). To study the morphological changes induced in single astrocytes expressing Epac1-camps, we analyzed the shape of cells (cell cross-sectional area and perimeter) before and within 30 min to 1 h after stimulation with different adrenergic receptor agonists and antagonists (Fig. 4), although these occurred in the majority of cells studied after the application of ligands. Both membrane-permeable cAMP-increasing reagents and β-AR agonists induced changes in astrocyte morphology, such as reduction in the cell cross-sectional area and the appearance of multiple sprouts, protrusions, and elongated processes on the membrane surface (Fig. 4). The cell cross-section area was changed by −0.0 ± 1.2% (Control; n = 15), 20.2 ± 3.1% (FSK; n = 5), 15.2 ± 7.8% (FSK + IBMX; n = 7), 8.0 ± 3.2% (db-cAMP; n = 8), 7.2 ± 1.6% (ADR; n = 9), −2.4 ± 2.3% (Pro + ADR; n = 10), 5.8 ± 3.5% (NA; n = 12), 4.4 ± 2.0% (Iso; n = 6). The cell perimeter was increased by 8.1 ± 3.4% (Control; n = 15), 54.4 ± 6.9% (FSK; n = 5), 27.1 ± 6.7% (FSK + IBMX; n = 7), 16.6 ± 4.5% (db-cAMP; n = 8), 44.3 ± 10.3% (ADR; n = 9), 6.5 ± 3.7% (Pro + ADR; n = 10), 32.8 ± 9.9% (NA; n = 12), and 32.8 ± 6.7% (Iso; n = 6) (Fig. 5). Stimulation of the cells with extracellular solution (control) did not trigger significant morphological changes compared with the other reagents (Figs. 4a and 5). Pre-

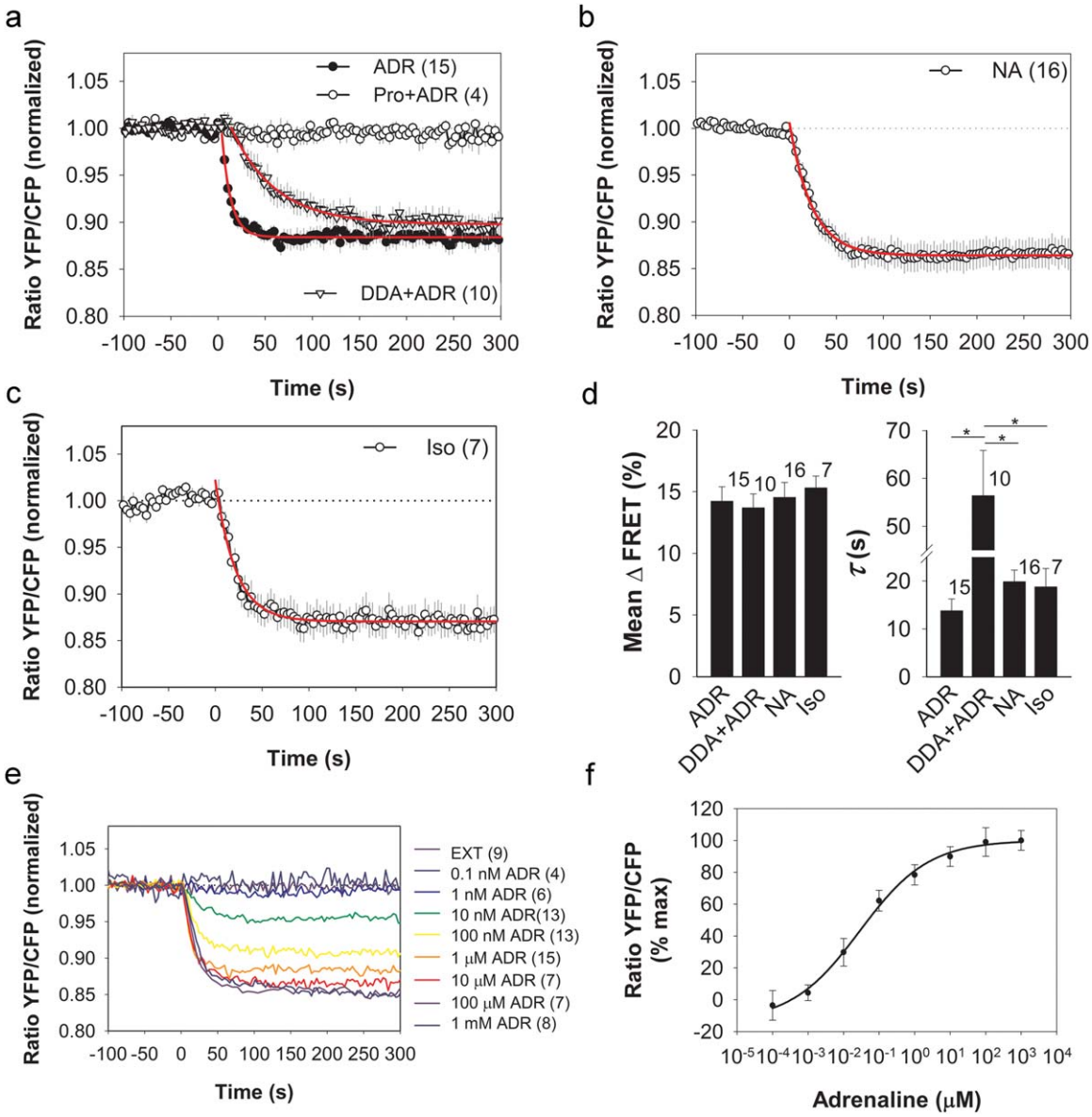

FIGURE 3: AR agonists increase intracellular cAMP levels in astrocytes in a concentration-dependent manner. (a–c) The time course of the Epac1-camps emission ratio after the addition of 1 μM ADR (t = 0) in the absence (black circle) and presence (white circle) of 1 μM Pro, a β-adrenergic antagonist and 100 μM DDA (down triangle), and after the addition of (b) 1 μM NA and (c) 1 μM Iso, a β-adrenergic agonist (t = 0). Note that the ADR-triggered FRET response exhibited slower decay kinetics in the presence of DDA and is completely prevented in the presence of Pro. (d) The mean amplitude of the changes in Epac1-camps FRET (left) and the mean decay time constants τ (right) for ADR, DDA + ADR, NA, and Iso. Changes in FRET are expressed as percentages relative to the initial values. $^{*}P < 0.05$ one-way ANOVA comparison between different types of stimuli. (e) Representative time course of Epac1-camps emission ratios on the addition of different concentrations of ADR. (f) Dose–response relationship between the maximum increase in cAMP (represented as the maximum YFP/CFP ratio) and ADR. The concentration of ADR at which 50% of the maximum cAMP increase was observed (EC_{50}) is 29 $\pm$ 0.10 nM. Data in (a–c, e) are expressed as the YFP/CFP fluorescence emission ratio normalized to the average baseline ratio values (ratio YFP/CFP). Numbers in parentheses depict the number (n) of independent experiments. Each data point represents the mean $\pm$ SEM of n independent experiments.

incubation of cells with Pro, a specific antagonist of β-AR, prevented the occurrence of ADR-induced changes in astrocyte morphology, indicating that the changes induced by ADR are mediated via β-AR signaling (Figs. 4f and 5). The analysis revealed a positive correlation between the cell cross-section area decrease and the cell perimeter increase that were induced by various afore-mentioned stimuli (y [% increase in cell perimeter] = [19.08 $\pm$ 3.75] + [1.53 $\pm$ 0.36] $\times$ x [% decrease in cell cross-section area], correlation coefficient [r] = 0.595, $P < 0.001$, n = 35, Fig. 5e) and bell-shaped

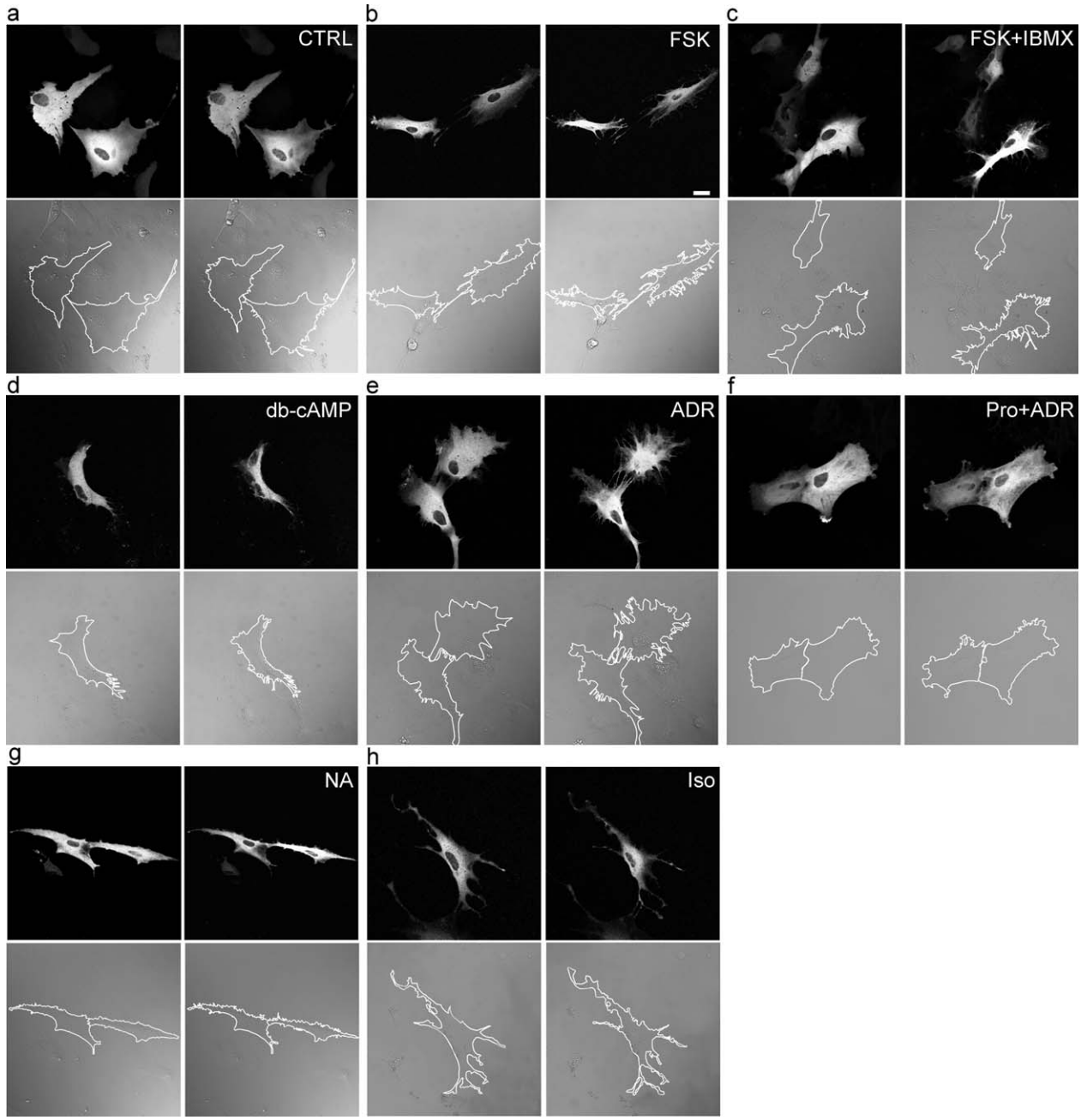

FIGURE 4: Increase in intracellular cAMP levels induces rapid changes in the cross-sectional area and perimeter of astrocytes. (a–h): Representative images of Epac1-camps transfected astrocytes (above) and their corresponding DIC images (below) before (left) and within 30 min to 1 h after (right) the addition of (a) extracellular solution (CTRL), (b) FSK, (c) FSK + IBMX, (d) db-cAMP, (e) ADR, (f) Pro + ADR, (g) NA, and (h) Iso. The perimeter of individual cells expressing Epac1-camps was traced using LSM510 META software, which also outlines the cross-sectional area of the cell. Scale bar: 20 μm.

relationship between the maximum YFP/CFP emission ratio response *versus* the decrease in cell cross-sectional area (Fig. 5c; $n = 35$) and the increase in cell perimeter (Fig. 5d, $n = 35$).

Discussion

We investigated the dynamics of intracellular cAMP levels, which are important in the control of many functions of astrocytes, including their morphological properties. The aim was to directly visualize the consequences of activation of β-ARs, which control cellular effectors via the cAMP signaling pathways, and the morphological changes. To monitor $[cAMP]_i$, we used the FRET-based cAMP sensor Epac1-camps (Nikolaev et al., 2004). The results revealed that the sensor reliably measures activation of the β-AR/cAMP

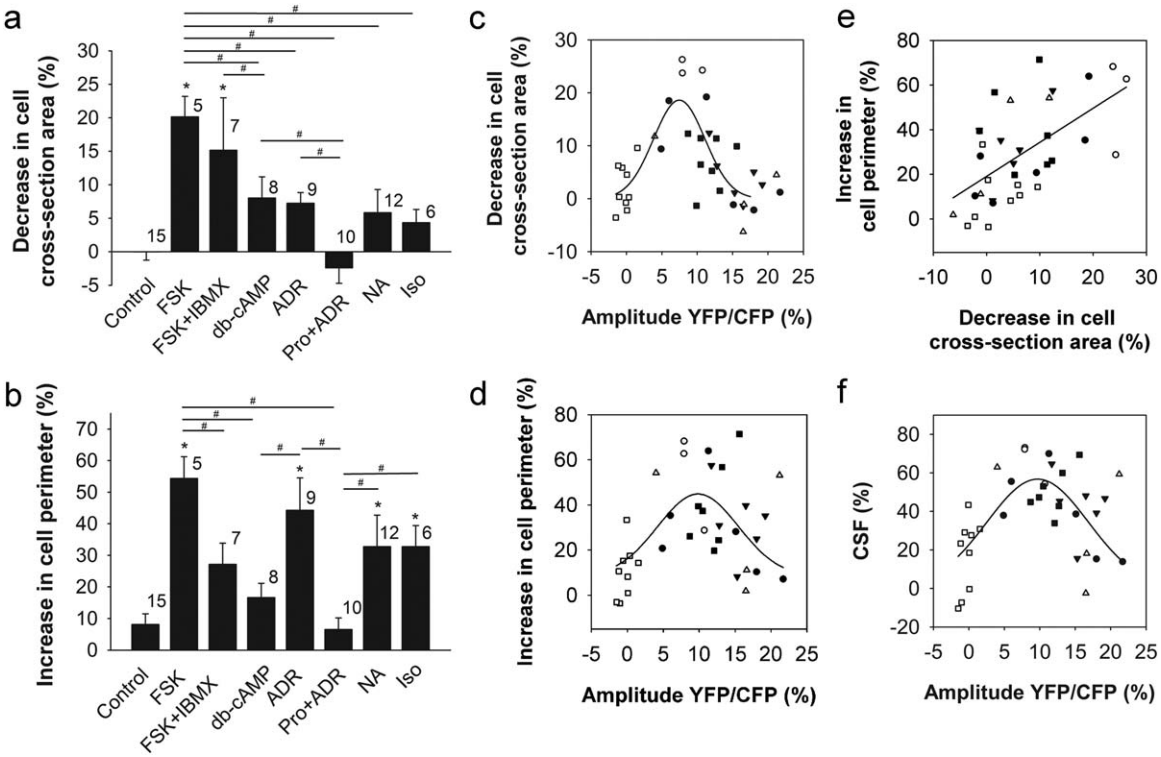

FIGURE 5: cAMP-increasing agents decrease the cross-sectional area and increase the perimeter of astrocytes. (a, b) Mean effect of extracellular solution (Control), FSK, FSK + IBMX, db-cAMP, ADR, Pro + ADR, NA, and Iso on the cell cross-sectional area (a) and perimeter (b) in Epac1-camps transfected astrocytes. Bars represent the mean ± SEM. *$P < 0.05$ one-way ANOVA comparison to control, ##$P < 0.05$ one-way ANOVA comparison between different types of stimuli. (c, d) Relationship between the amplitude of the YFP/CFP ratio *versus* (c) the decrease in cell cross-sectional area and (d) the increase in the cell perimeter. (e) Relationship between the relative decrease in cell cross-section area and the relative increase in cell perimeter. The line represents linear fit to the data with the slope $b = 1.53 \pm 0.36$ ($P < 0.001$), with the intercept $a = 19.08 \pm 3.75$ ($P < 0.0001$) and r the correlation coefficient of 0.595 ($P < 0.01$, $n = 35$). (f) Relationship between the amplitude of the YFP/CFP ratio *versus* the CSF. Note that the relationship between the amplitude of YFP/CFP and the changes in (c) the cross-sectional area, (d) perimeter, and (f) CSF exhibits a bell-shaped curve; see Materials and Methods section for the Gaussian equation fitted to the data in (c),(d), and (f); the parameters in (c) were $y = (18.62 \pm 2.55) \times \exp(-0.5 \times ((x - (7.47 \pm 0.55))/(3.63 \pm 0.52))^2)$, in (d) were $y = (43.47 \pm 5.42) \times \exp(-0.5 \times ((x - 10.17 \pm 1.13)/(7.03 \pm 1.22))^2)$, and in (f) were $y = (56.74 \pm 5.57) \times \exp(-0.5 \times ((x - (9.71 \pm 0.87))/(7.16 \pm 0.96))^2)$. Control (white squares), FSK (white circles), FSK + IBMX (black circles), ADR (black squares), NA (triangles), and Iso (black down triangles).

signaling pathway in astrocytes and that this novel real-time approach can be used to follow morphological changes during astrocyte stellation.

Tonic Activities of AC and PDE Determine Basal cAMP Levels in Astrocytes

Intracellular $[cAMP]_i$ represents the net balance between the synthesis and degradation of cAMP mainly by two enzymes, AC and PDE, respectively (Baillie, 2009). To monitor real-time changes in $[cAMP]_i$ in single living astrocytes, imaging experiments with the FRET-based cAMP sensor, Epac1-camps, were performed. Expression of Epac1-camps in astrocytes showed a uniform distribution throughout the cytosol, but was excluded from the nucleus in the majority of cells, consistent with the expression of the sensor in other cells, that is, Chinese hamster ovary cells, mouse primary neurons, peritoneal macrophages, and MIN6 β-cells (Landa et al., 2005; Nikolaev et al., 2004). Direct stimulation of AC with FSK, independently of GPCR and G_s signaling, induced an increase in $[cAMP]_i$ in astrocytes, with the time constant of ~40 s. When the cyclic nucleotide-degrading enzyme PDE was inhibited by IBMX, the increase in cAMP levels on FSK stimulation was ~40% greater than in cells stimulated with FSK only. Thus, in astrocytes, cAMP is constantly being degraded due to tonic activity of PDEs. The AC inhibitor, DDA, suppressed basal cAMP levels in 50% of DDA-treated cells, suggesting that AC is constitutively active in astrocytes. This is consistent with the results observed in Epac1-camps expressing cardiomyocytes treated with the AC inhibitor MDL-12,330A hydrochloride (Börner et al., 2011). In 50% of DDA-treated astrocytes, no significant change in FRET signal was observed. In these cells, the basal $[cAMP]_i$ is likely $\leq$100 nM (Börner et al., 2011) and thus changes in the FRET signal on DDA treatment are not in the sensitivity

range of the Epac1-camps sensor. As in MIN6 β-cells (Landa et al., 2005), we have observed heterogeneity of the intensity of the Epac1-camps FRET emission between transfected astrocytes. The observed differences in FRET response in DDA-treated cells and the heterogeneity of the intensity of the Epac1-camps FRET emission suggest variability in the basal $[cAMP]_i$ between astrocytes in culture.

β-AR Stimulation Rapidly Increases $[cAMP]_i$ in Astrocytes, But There Are No Oscillations

β-AR/cAMP signaling has been shown to be linked to many important functions of both resting and reactive astrocytes in the brain (Sutin and Shao, 1992), therefore it is important to understand the temporal dynamics of β-AR/cAMP signaling in astrocytes. Using biochemical methods to detect cAMP, it has been reported that activation of β-ARs on the surface of astrocytes results in a transient increase in the intracellular cAMP level, which reaches a maximum ∼5 min after receptor activation and then slowly declines to control levels (Shain et al., 1987). However, in contrast, our real-time FRET imaging of change in cAMP on β-AR activation in astrocytes using the Epac1-camps sensor revealed that β-AR agonists (selective and nonselective) induced an increase in $[cAMP]_i$ with a time constant of ∼15 s. Thus, rapid coupling of β-AR activation with the production of intracellular cAMP by AC is evident from these experiments. Although stimulation of β-AR activates AC indirectly through GPCR/G_s, the FRET response was twofold faster in astrocytes stimulated with β-AR agonists than in FSK-stimulated cells. This may be due to the slow membrane permeability of FSK and/or its slow activation of AC. Consistent with this, the cAMP analog db-cAMP, which is also slow in crossing the plasma membrane and in hydrolyzing into the active form (Schultz et al., 1994; Zhang et al., 2001), induced >35-fold slower FRET response than β-AR agonists.

The ADR-induced increase in $[cAMP]_i$ was dose dependent with a half-maximum FRET response at 30 nM ADR, consistent with the high affinity of astrocytic β-AR for ADR. This value is comparable with the EC_{50} values obtained for Iso and NA in Epac1-camps expressing adult cardiomyocytes (Nikolaev et al., 2004). The β-AR antagonist Pro completely prevented the ADR-induced increase in $[cAMP]_i$. Moreover, in astrocytes expressing the PKA-based cAMP sensor AKAR2, the ADR-induced increase in $[cAMP]_i$ was inhibited by the addition of the β-AR antagonist Pro (data not shown), excluding the participation of astrocytic α-ARs in the ADR-induced increase in $[cAMP]_i$. In DDA-treated astrocytes, the FRET response, reporting changes in $[cAMP]_i$ on ADR stimulation, was fourfold slower compared with controls. Thus, AC is directly linked to the β-adrenergic signaling pathway in astrocytes. These results clearly show that astrocytes respond to agonist-induced β-AR stimulation in a rapid concentration-dependent manner through G_s/AC activation. The fastest change in $[cAMP]_i$ recorded after the activation of β-AR occurs within 15 s in these experiments.

These measurements revealed that once $[cAMP]_i$ attained a steady state, we observed no oscillations, although they have been predicted in previous modeling studies (Cooper et al., 1995) and by measurements in other cell types (Willoughby and Cooper, 2006). Therefore, cAMP in astrocytes likely controls cellular processes in a relatively slow time domain compared with the other second messenger Ca^{2+}, where relatively rapid oscillations in $[Ca^{2+}]_i$ have been measured (Parpura et al., 2012).

β-AR Stimulation Elicits Astrocyte Rapid Stellate Morphology

Although astrocytes in culture have flattened polygonal morphology, they may transform on activation of the β-AR/cAMP pathway via a series of cytoskeletal reorganizations, which include the restructuring of actin filaments, microtubules, and intermediate filaments (Goldman and Abramson, 1990; Safavi-Abbasi et al., 2001), into stellate, process-bearing cells (Bicknell et al., 1989; Gharami and Das, 2004; Hatton et al., 1991; Shain et al., 1987; Shao et al., 1994; Won and Oh, 2000). These cells resemble the stellate morphology of reactive tissue astrocytes. Using the Epac1-camps cAMP sensor, the results show that astrocytes attain stellate morphology within 1 h on β-AR activation (Figs. 4 and 5), consistent with previous studies (Gharami and Das, 2004; Shain et al., 1987). In the majority of cells, small changes in morphology were detected immediately after β-AR stimulation [data not shown; (Shain et al., 1987)]. The treatment of astrocytes with FSK and db-cAMP induced similar morphological changes to those observed with β-AR agonists, indicating that these morphological changes are cAMP dependent (Shain et al., 1987). FSK response was stronger compared with that observed with db-cAMP and β-AR agonists (Fig. 5). FSK permeates plasma membrane and activates all available ACs inside the cell. This likely affects a stronger decrease in the cell cross-section area and the increase in cell perimeter in comparison to β-AR agonists, which activate only ACs linked to the plasma membrane resident β-AR receptors. The weaker effect of db-cAMP on morphological changes may be due to slow crossing of db-cAMP across the plasma membrane and the fact that db-cAMP needs to be hydrolyzed into its active form before binding to its effectors (Schultz et al., 1994; Zhang et al., 2001). Pretreatment of astrocytes with Pro prevented ADR-induced astrocyte stellation, thus excluding the involvement of α-ARs in stellation. A reduction in the cell cross-sectional area of 5–20% was measured,

TABLE 1.: Morphometric Analysis of Astrocyte Shapes Before and After Stimulation by cAMP-Elevating Agents

Type of stimulus	CSF Before stimulation	CSF After stimulation	Decrease in CSF (%)	*n*
Control	0.218 ± 0.020	0.198 ± 0.023	10.8 ± 5.5	15
FSK (50 μM)	0.137 ± 0.025	0.047 ± 0.009	65.7 ± 3.4**	5
FSK + IBMX (50 μM + 200 μM)	0.194 ± 0.045	0.120 ± 0.038	43.7 ± 9.2**	7
db-cAMP (1 mM)	0.186 ± 0.037	0.126 ± 0.024	30.2 ± 6.3*	8
ADR (1 μM)	0.193 ± 0.026	0.094 ± 0.017	51.0 ± 5.4**	9
Pro + ADR (1 μM+1 μM)	0.253 ± 0.036	0.226 ± 0.028	7.1 ± 6.1	10
NA (1 μM)	0.244 ± 0.028	0.142 ± 0.023	38.3 ± 7.7**	12
Iso (1 μM)	0.195 ± 0.032	0.119 ± 0.030	43.3 ± 6.5*	6

CSF was calculated according to the equation: $4\pi A/P^2$, where A is the cell cross-section area and P the cell perimeter. This measure ranges from 0 to 1 between extremes of a line and a perfect circle (one-way ANOVA compared with control. $^{**}P < 0.001$, $^{*}P < 0.05$). *n* denotes the number of experiments. FSK: forskolin; IBMX: 3-isobutyl-l-methylxanthine; db-cAMP: dibutyryl-cAMP; ADR: adrenaline; NA: noradrenaline; Iso: isoprenaline; Pro: propranolol.

suggesting the withdrawal of cytoplasm to the perinuclear region due to restructuring of the cytoskeleton (Shain et al., 1987). The cell perimeter increased by 30–50% with concomitant appearance of short sprouts on the plasma membrane with some elongated processes. We observed a positive correlation between the cell cross-section area decrease and the cell perimeter and a bell-shaped relationship between the FRET signal reporting $[cAMP]_i$ and changes in cell cross-sectional area and perimeter. These results indicate that within 1 h after β-AR stimulation, which increases $[cAMP]_i$, important morphological changes in the cell cross-sectional area and perimeter are observed.

To address the stellation of astrocytes in a more quantitative way, we calculated the cell shape factor (CSF = $4\pi A/P^2$; where A is cell cross-section area and P is cell perimeter; Table 1., Fig. 5f). The CSF of a perfect circle equals 1. In contrast, thread-like objects exhibit a CSF approaching 0. Therefore, perfectly round cells have a shape factor close to 1, whereas more elongated or star-like cells (with a large number of long filopodia) exhibit lower values (Burgstaller et al., 2010; Cohen and Fields, 2008). The changes in CSF, expressed as the percent reductions in CSF, relative to the CSF before the treatment by FSK, FSK + IBMX, and db-cAMP, were three- to sixfolds larger than in controls; 65.7% (FSK), 43.7% (FSK + IBMX), and 30.2% (db-cAMP) *versus* 10.8% (Control). Similar decreases in CSF were observed in cells upon β-AR stimulation; 51.0% (ADR), 38.3% (NA), and 43.3% (Iso). The decrease in CSF upon ADR application in the presence of Pro was only 7.1%, not significantly different than controls (Table 1.). A bell-shaped relationship between the FRET signal reporting $[cAMP]_i$ and CSF was observed (Fig. 5f). These quantitative morphometry analyses support the conclusion that in astrocytes β-AR agonists induce stellation within less than 1 h after the application of stimuli.

The observation that β-AR activation induces transient increases in cAMP, which decay towards control levels after reaching a peak in ~5 min (Shain et al., 1987), suggests that cAMP might only be involved in the early stages of β-AR-induced transformation of astrocytes. β-AR agonists and FSK increase intracellular PKA activity (unpublished), indicating that the increase in $[cAMP]_i$ induced by various cAMP-elevating agents is followed by the activation of cAMP-dependent PKA. It was reported that the morphological changes induced by continuous β-AR activation progress over time and reach their maximum after 48 h, however β-AR stimulation affects the activity of cAMP-dependent PKA only for up to 2 h, thus indicating the involvement of downstream regulators of the β-AR/cAMP pathway in the regulation of the late stages of astrocyte stellation (Gharami and Das, 2004). Delayed and sustained activation of mitogen-activated protein kinase p-ERK (phosphorylated extracellular signal-regulated kinase) has been proposed to be critical for the later stages of β-AR-induced transformation of astrocytes (Gharami and Das, 2004). In accordance with this, astrocyte stellation was recently shown to depend not only on cAMP levels but also on Rac1, a small GTPase of the Rho family, and its effector ROCK (Racchetti et al., 2012).

Pathophysiologic Significance of cAMP-Mediated Astrocyte Morphology Changes

In vivo astrocytes in the CNS respond to different pathologic conditions such as trauma, ischemia, infection, inflammation, neurodegeneration by becoming reactive, which may lead to

reactive gliosis. In this state astrocytes, also termed reactive astrocytes, exhibit hypertrophic morphology with prominent processes (Wilhelmsson et al., 2006). These morphological characteristics resemble the cAMP-induced morphological changes observed in cultured astrocytes (Fig. 4). *In vivo* blockade of β-AR suppresses reactive gliosis (Griffith and Sutin, 1996; Sutin and Griffith, 1993), indicating the involvement of noradrenergic stimulation and cAMP signaling in the transformation of resting astrocytes into reactive astrocytes. Locus coeruleus is the main site of NA synthesis in the brain and noradrenergic neurons from this nucleus innervate almost all brain areas. In early stages of Alzheimer's disease (Hammerschmidt et al., 2013) and in multiple sclerosis (Polak et al., 2011) degeneration of locus coeruleus occurs leading to the loss of cortical noradrenergic innervation and a reduction of NA, which affects β-AR/cAMP signaling in the brain and consequently also astrocyte morphology. Consistent with this astrocyte atrophy was reported in some parts of the brain in the early stages of Alzheimer's disease (Olabarria et al., 2010).

Recent studies indicate that in the CNS, glial morphology could be dynamically regulated by the release of neurotransmitters, affecting cAMP signaling, from surrounding cells. β-AR/cAMP-triggered stellation of cultured astrocytes can be blocked by neurotransmitter glutamate (Shao et al., 1994; Won and Oh, 2000) and in embryonic astrocytes by ATP (Abe and Saito, 1999). The cAMP signaling pathway was also shown to mediate inhibition of hypotonic swelling in retinal glial cells in mice by ATP and adenosine (Wurm et al., 2009, 2010). Because astrocyte processes ensheath neurons, rapid cAMP-mediated local retractions, or expansions of the astrocyte processes that modify the geometry of the extracellular space at the tripartite synapse may affect neuronal and astrocytic excitability (Theodosis et al., 2008). This may play an important role not only in physiology but also in the pathology of the CNS, in particular during edema and reactive gliosis, when astrocytes undergo morphological changes such as cell swelling and stellation. Moreover, in addition to proliferation, astrocytes also exhibit morphological changes *in vivo* in acute injury (Bardehle et al., 2013), which may involve changes in cAMP levels, as measured in our study.

cAMP imaging has been recently performed in living vertebrate neuronal tissue using a neuron-specific cAMP probe based on Epac1-camps (Mironov et al., 2009). In future, the expression of fluorescent cAMP nanosensors under astrocyte-restricted promoters *in vivo* would help us to understand how β-AR/cAMP-dependent signaling mechanisms, which underlie changes in astrocyte morphology and modulations in astrocyte excitability, metabolism, and so forth, operate in connection with other residential brain cells.

In summary, our results show that the activation of β-AR rapidly increases $[cAMP]_i$ to a steady state level, which affects the morphology of astrocytes. The relationship between the FRET signal reporting $[cAMP]_i$ and changes in the cell cross-sectional area and perimeter exhibited a bell-shaped curve, indicating that maximal morphological changes are limited to an optimal (narrow) range of $[cAMP]_i$.

Acknowledgment

Grant sponsor: Slovenian Research Agency (ARRS); Grant numbers: P3 310, J3 4051, J3 3632, J3 4146 and J3 5499; Grant sponsor: CipKeBip; Grant sponsor: EC; Grant number: EDuGlia ITN EU.

The authors thank Dr. Martin Lohse and Dr. Viacheslav Olegowitsch Nikolaev for providing the Epac1-camps FRET plasmid. The authors thank Zala Lužnik and Urša Gubenšek for support with the experiments.

References

Abe K, Saito H. 1999. Effect of ATP on astrocyte stellation is switched from suppressive to stimulatory during development. Brain Res 850:150–157.

Allaman I, Lengacher S, Magistretti PJ, Pellerin L. 2003. A2B receptor activation promotes glycogen synthesis in astrocytes through modulation of gene expression. Am J Physiol Cell Physiol 284:C696–704.

Aoki C. 1992. Beta-adrenergic receptors: Astrocytic localization in the adult visual cortex and their relation to catecholamine axon terminals as revealed by electron microscopic immunocytochemistry. J Neurosci 12:781–792.

Baillie GS. 2009. Compartmentalized signalling: Spatial regulation of cAMP by the action of compartmentalized phosphodiesterases. FEBS J 276:1790–1799.

Balázs R, Miller S, Chun Y, O'Toole J, Cotman CW. 1998. Metabotropic glutamate receptor agonists potentiate cyclic AMP formation induced by forskolin or beta-adrenergic receptor activation in cerebral cortical astrocytes in culture. J Neurochem 70:2446–2458.

Bardehle S, Krüger M, Buggenthin F, Schwausch J, Ninkovic J, Clevers H, Snippert HJ, Theis FJ, Meyer-Luehmann M, Bechmann I, Dimou L, Götz M. 2013. Live imaging of astrocyte responses to acute injury reveals selective juxtavascular proliferation. Nat Neurosci 16:580–586.

Beavo JA, Brunton LL. 2002. Cyclic nucleotide research—Still expanding after half a century. Nat Rev Mol Cell Biol 3:710–718.

Bicknell RJ, Luckman SM, Inenaga K, Mason WT, Hatton GI. 1989. Beta-adrenergic and opioid receptors on pituicytes cultured from adult rat neurohypophysis: Regulation of cell morphology. Brain Res Bull 22:379–388.

Bolton S, Greenwood K, Hamilton N, Butt AM. 2006. Regulation of the astrocyte resting membrane potential by cyclic AMP and protein kinase A. Glia 54:316–328.

Börner S, Schwede F, Schlipp A, Berisha F, Calebiro D, Lohse MJ, Nikolaev VO. 2011. FRET measurements of intracellular cAMP concentrations and cAMP analog permeability in intact cells. Nat Protoc 6:427–438.

Burgstaller G, Gregor M, Winter L, Wiche G. 2010. Keeping the vimentin network under control: Cell-matrix adhesion-associated plectin 1f affects cell shape and polarity of fibroblasts. Mol Biol Cell 21:3362–3375.

Catus SL, Gibbs ME, Sato M, Summers RJ, Hutchinson DS. 2011. Role of β-adrenoceptors in glucose uptake in astrocytes using β-adrenoceptor knockout mice. Br J Pharmacol 162:1700–1715.

Ciccarelli R, D'Alimonte I, Ballerini P, D'Auro M, Nargi E, Buccella S, Di Iorio P, Bruno V, Nicoletti F, Caciagli F. 2007. Molecular signalling mediating the protective effect of A1 adenosine and mGlu3 metabotropic glutamate receptor activation against apoptosis by oxygen/glucose deprivation in cultured astrocytes. Mol Pharmacol 71:1369–1380.

Cohen JE, Fields RD. 2008. Activity-dependent neuron-glial signaling by ATP and leukemia-inhibitory factor promotes hippocampal glial cell development. Neuron Glia Biol 4:43–55.

Cooper DM, Mons N, Karpen JW. 1995. Adenylyl cyclases and the interaction between calcium and cAMP signalling. Nature 374:421–424.

de Rooij J, Zwartkruis FJ, Verheijen MH, Cool RH, Nijman SM, Wittinghofer A, Bos JL. 1998. Epac is a Rap1 guanine-nucleotide-exchange factor directly activated by cyclic AMP. Nature 396:474–477.

DiPilato LM, Cheng X, Zhang J. 2004. Fluorescent indicators of cAMP and Epac activation reveal differential dynamics of cAMP signaling within discrete subcellular compartments. Proc Natl Acad Sci USA 101:16513–16518.

Durand D, Carniglia L, Caruso C, Lasaga M. 2011. Reduced cAMP, Akt activation and p65-c-Rel dimerization: Mechanisms involved in the protective effects of mGluR3 agonists in cultured astrocytes. PLoS One 6:e22235.

Gharami K, Das S. 2004. Delayed but sustained induction of mitogen-activated protein kinase activity is associated with beta-adrenergic receptor-mediated morphological differentiation of astrocytes. J Neurochem 88:12–22.

Goldman JE, Abramson B. 1990. Cyclic AMP-induced shape changes of astrocytes are accompanied by rapid depolymerization of actin. Brain Res 528:189–196.

Griffith R, Sutin J. 1996. Reactive astrocyte formation in vivo is regulated by noradrenergic axons. J Comp Neurol 371:362–375.

Guček A, Vardjan N, Zorec R. 2012. Exocytosis in astrocytes: Transmitter release and membrane signal regulation. Neurochem Res 37:2351–2363.

Hammerschmidt T, Kummer MP, Terwel D, Martinez A, Gorji A, Pape HC, Rommelfanger KS, Schroeder JP, Stoll M, Schultze J, Weinshenker D, Heneka MT. 2013. Selective loss of noradrenaline exacerbates early cognitive dysfunction and synaptic deficits in APP/PS1 mice. Biol Psychiatry 73:454–463.

Hatton GI, Luckman SM, Bicknell RJ. 1991. Adrenalin activation of beta 2-adrenoceptors stimulates morphological changes in astrocytes (pituicytes) cultured from adult rat neurohypophyses. Brain Res Bull 26:765–769.

Kanno T, Nishizaki T. 2012. A(2a) adenosine receptor mediates PKA-dependent glutamate release from synaptic-like vesicles and Ca efflux from an IP(3)- and ryanodine-insensitive intracellular calcium store in astrocytes. Cell Physiol Biochem 30:1398–1412.

Kreft M, Bak LK, Waagepetersen HS, Schousboe A. 2012. Aspects of astrocyte energy metabolism, amino acid neurotransmitter homoeostasis and metabolic compartmentation. ASN Neuro 4.

Landa LR, Harbeck M, Kaihara K, Chepurny O, Kitiphongspattana K, Graf O, Nikolaev VO, Lohse MJ, Holz GG, Roe MW. 2005. Interplay of Ca2+ and cAMP signaling in the insulin-secreting MIN6 beta-cell line. J Biol Chem 280: 31294–31302.

Laureys G, Clinckers R, Gerlo S, Spooren A, Wilczak N, Kooijman R, Smolders I, Michotte Y, De Keyser J. 2010. Astrocytic beta(2)-adrenergic receptors: From physiology to pathology. Prog Neurobiol 91:189–199.

Lee RK, Araki W, Wurtman RJ. 1997. Stimulation of amyloid precursor protein synthesis by adrenergic receptors coupled to cAMP formation. Proc Natl Acad Sci USA 94:5422–5426.

Lim R, Mitsunobu K, Li WK. 1973. Maturation-stimulation effect of brain extract and dibutyryl cyclic AMP on dissociated embryonic brain cells in culture. Exp Cell Res 79:243–246.

Mironov SL, Skorova E, Taschenberger G, Hartelt N, Nikolaev VO, Lohse MJ, Kügler S. 2009. Imaging cytoplasmic cAMP in mouse brainstem neurons. BMC Neurosci 10:29.

Nikolaev VO, Bünemann M, Hein L, Hannawacker A, Lohse MJ. 2004. Novel single chain cAMP sensors for receptor-induced signal propagation. J Biol Chem 279:37215–37218.

Nikolaev VO, Bünemann M, Schmitteckert E, Lohse MJ, Engelhardt S. 2006. Cyclic AMP imaging in adult cardiac myocytes reveals far-reaching beta1-adrenergic but locally confined beta2-adrenergic receptor-mediated signaling. Circ Res 99:1084–1091.

Norris JG, Benveniste EN. 1993. Interleukin-6 production by astrocytes: Induction by the neurotransmitter norepinephrine. J Neuroimmunol 45:137–145.

Olabarria M, Noristani HN, Verkhratsky A, Rodríguez JJ. 2010. Concomitant astroglial atrophy and astrogliosis in a triple transgenic animal model of Alzheimer's disease. Glia 58:831–838.

Parpura V, Heneka MT, Montana V, Oliet SH, Schousboe A, Haydon PG, Stout RF, Spray DC, Reichenbach A, Pannicke T, Pekny M, Pekna M, Zorec R, Verkhratsky A. 2012. Glial cells in (patho)physiology. J Neurochem 121:4–27.

Polak PE, Kalinin S, Feinstein DL. 2011. Locus coeruleus damage and noradrenaline reductions in multiple sclerosis and experimental autoimmune encephalomyelitis. Brain 134:665–677.

Prebil M, Jensen J, Zorec R, Kreft M. 2011a. Astrocytes and energy metabolism. Arch Physiol Biochem 117:64–69.

Prebil M, Vardjan N, Jensen J, Zorec R, Kreft M. 2011b. Dynamic monitoring of cytosolic glucose in single astrocytes. Glia 59:903–913.

Racchetti G, D'Alessandro R, Meldolesi J. 2012. Astrocyte stellation, a process dependent on Rac1 is sustained by the regulated exocytosis of enlargeosomes. Glia 60:465–475.

Rathbone MP, Middlemiss PJ, DeLuca B, Jovetich M. 1991. Extracellular guanosine increases astrocyte cAMP: Inhibition by adenosine A2 antagonists. Neuroreport 2:661–664.

Rich TC, Tse TE, Rohan JG, Schaack J, Karpen JW. 2001. In vivo assessment of local phosphodiesterase activity using tailored cyclic nucleotide-gated channels as cAMP sensors. J Gen Physiol 118:63–78.

Rosenberg PA, Li Y. 1995. Adenylyl cyclase activation underlies intracellular cyclic AMP accumulation, cyclic AMP transport, and extracellular adenosine accumulation evoked by beta-adrenergic receptor stimulation in mixed cultures of neurons and astrocytes derived from rat cerebral cortex. Brain Res 692:227–232.

Roy ML, Sontheimer H. 1995. Beta-adrenergic modulation of glial inwardly rectifying potassium channels. J Neurochem 64:1576–1584.

Safavi-Abbasi S, Wolff JR, Missler M. 2001. Rapid morphological changes in astrocytes are accompanied by redistribution but not by quantitative changes of cytoskeletal proteins. Glia 36:102–115.

Schultz C, Vajanaphanich M, Genieser HG, Jastorff B, Barrett KE, Tsien RY. 1994. Membrane-permeant derivatives of cyclic AMP optimized for high potency, prolonged activity, or rapid reversibility. Mol Pharmacol 46:702–708.

Schwartz JP, Nishiyama N. 1994. Neurotrophic factor gene expression in astrocytes during development and following injury. Brain Res Bull 35:403–407.

Schwartz J, Wilson D. 1992. Preparation and characterization of type 1 astrocytes cultured from adult rat cortex, cerebellum, and striatum. Glia 5:75–80.

Shain W, Forman DS, Madelian V, Turner JN. 1987. Morphology of astroglial cells is controlled by beta-adrenergic receptors. J Cell Biol 105:2307–2314.

Shao Y, Enkvist MO, McCarthy KD. 1994. Glutamate blocks astroglial stellation: Effect of glutamate uptake and volume changes. Glia 11:1–10.

Shapiro DL. 1973. Morphological and biochemical alterations in foetal rat brain cells cultured in the presence of monobutyryl cyclic AMP. Nature 241: 203–204.

Sorg O, Magistretti PJ. 1992. Vasoactive intestinal peptide and noradrenaline exert long-term control on glycogen levels in astrocytes: Blockade by protein synthesis inhibition. J Neurosci 12:4923–4931.

Sutherland EW, Rall TW. 1960. Formation of adenosine-3,5-phosphate (cyclic adenylate) and its relation to the action of several neurohormones or hormones. Acta Endocrinol Suppl (Copenh) 34(Suppl 50):171–174.

Sutin J, Griffith R. 1993. Beta-adrenergic receptor blockade suppresses glial scar formation. Exp Neurol 120:214–222.

Sutin J, Shao Y. 1992. Resting and reactive astrocytes express adrenergic receptors in the adult rat brain. Brain Res Bull 29:277–284.

Theodosis DT, Poulain DA, Oliet SH. 2008. Activity-dependent structural and functional plasticity of astrocyte-neuron interactions. Physiol Rev 88:983–1008.

Wilhelmsson U, Bushong EA, Price DL, Smarr BL, Phung V, Terada M, Ellisman MH, Pekny M. 2006. Redefining the concept of reactive astrocytes as cells that remain within their unique domains upon reaction to injury. Proc Natl Acad Sci USA 103:17513–17518.

Willoughby D, Cooper DM. 2006. Ca2+ stimulation of adenylyl cyclase generates dynamic oscillations in cyclic AMP. J Cell Sci 119:828–836.

Willoughby D, Cooper DM. 2008. Live-cell imaging of cAMP dynamics. Nat Methods 5:29–36.

Won CL, Oh YS. 2000. cAMP-induced stellation in primary astrocyte cultures with regional heterogeneity. Brain Res 887:250–258.

Wurm A, Lipp S, Pannicke T, Linnertz R, Färber K, Wiedemann P, Reichenbach A, Bringmann A. 2009. Involvement of A(1) adenosine receptors in osmotic volume regulation of retinal glial cells in mice. Mol Vis 15:1858–1867.

Wurm A, Lipp S, Pannicke T, Linnertz R, Krügel U, Schulz A, Färber K, Zahn D, Grosse J, Wiedemann P, Chen J, Schöneberg T, Illes P, Reichenbach A, Bringmann A. 2010. Endogenous purinergic signaling is required for osmotic volume regulation of retinal glial cells. J Neurochem 112:1261–1272.

Yu N, Martin JL, Stella N, Magistretti PJ. 1993. Arachidonic acid stimulates glucose uptake in cerebral cortical astrocytes. Proc Natl Acad Sci USA 90: 4042–4046.

Zaccolo M, De Giorgi F, Cho CY, Feng L, Knapp T, Negulescu PA, Taylor SS, Tsien RY, Pozzan T. 2000. A genetically encoded, fluorescent indicator for cyclic AMP in living cells. Nat Cell Biol 2:25–29.

Zeinstra E, Wilczak N, De Keyser J. 2000. [3H]dihydroalprenolol binding to beta adrenergic receptors in multiple sclerosis brain. Neurosci Lett 289:75–77.

Zhang J, Hupfeld CJ, Taylor SS, Olefsky JM, Tsien RY. 2005. Insulin disrupts beta-adrenergic signalling to protein kinase A in adipocytes. Nature 437:569–573.

Zhang J, Ma Y, Taylor SS, Tsien RY. 2001. Genetically encoded reporters of protein kinase A activity reveal impact of substrate tethering. Proc Natl Acad Sci USA 98:14997–15002.

Zorec R, Araque A, Carmignoto G, Haydon PG, Verkhratsky A, Parpura V. 2012. Astroglial excitability and gliotransmission: An appraisal of Ca2+ as a signalling route. ASN Neuro 4.